Intensifying the Charging Response of a Phase-Change Material with Twisted Fin Arrays in a Shell-And-Tube Storage System

Mohammad Ghalambaz [1,2], Hayder I. Mohammed [3], Jasim M. Mahdi [4], Amir Hossein Eisapour [5], Obai Younis [6,7], Aritra Ghosh [8,9,10], Pouyan Talebizadehsardari [1,2,*] and Wahiba Yaïci [11,*]

1. Metamaterials for Mechanical, Biomechanical and Multiphysical Applications Research Group, Ton Duc Thang University, Ho Chi Minh City 758307, Vietnam; mohammad.ghalambaz@tdtu.edu.vn
2. Faculty of Applied Sciences, Ton Duc Thang University, Ho Chi Minh City 758307, Vietnam
3. Department of Physics, College of Education, University of Garmian, Kurdistan, Kalar 46021, Iraq; hayder.i.mohammad@garmian.edu.krd
4. Department of Energy Engineering, University of Baghdad, Baghdad 10071, Iraq; jasim@siu.edu
5. Department of Energy and Aerospace Engineering, School of Mechanical Engineering, Shiraz University, Shiraz 84334-71946, Iran; a.h.eisapour@gmail.com
6. Department of Mechanical Engineering, College of Engineering at Wadi Addwaser, Prince Sattam Bin Abdulaziz University, Wadi Addwaser 11991, Saudi Arabia; oubeytaha@hotmail.com
7. Department of Mechanical Engineering, Faculty of Engineering, University of Khartoum, Khartoum 11111, Sudan
8. Environment and Sustainability Institute, University of Exeter, Penryn, Cornwall TR10 9FE, UK; a.ghosh@exeter.ac.uk
9. College of Engineering, Mathematics and Physical Sciences, Renewable Energy, University of Exeter, Cornwall TR10 9FE, UK
10. Renewable Energy, Stella Turk Building, University of Exeter, Penryn, Cornwall TR10 9FE, UK
11. CanmetENERGY Research Centre, Natural Resources Canada, 1 Haanel Drive, Ottawa, ON K1A 1M1, Canada
* Correspondence: ptsardari@tdtu.edu.vn (P.T.); wahiba.yaici@canada.ca (W.Y.); Tel.: +1-613-996-3734 (W.Y.)

Abstract: A twisted-fin array as an innovative structure for intensifying the charging response of a phase-change material (PCM) within a shell-and-tube storage system is introduced in this work. A three-dimensional model describing the thermal management with charging phase change process in PCM was developed and numerically analyzed by the enthalpy-porosity method using commercial CFD software. Efficacy of the proposed structure of fins for performing better heat communication between the active heating surface and the adjacent layers of PCM was verified via comparing with conventional longitudinal fins within the same design limitations of fin material and volume usage. Optimization of the fin geometric parameters including the pitch, number, thickness, and the height of the twisted fins for superior performance of the proposed fin structure, was also introduced via the Taguchi method. The results show that a faster charging rate, higher storage rate, and better uniformity in temperature distribution could be achieved in the PCMs with Twisted fins. Based on the design of twisted fins, it was found that the energy charging time could be reduced by up to 42%, and the energy storage rate could be enhanced up to 63% compared to the reference case of straight longitudinal fins within the same PCM mass limitations.

Keywords: thermal storage; latent heat; phase change process; melting enhancement; twisted fins

1. Introduction

The excessive dependence on fossil fuels to meet humankind's hunger for energy has led to undesirable phenomena like global warming and environmental pollution. Therefore, the search for exploiting energy alternatives like solar and wind has become a key priority for researchers worldwide. The major challenge that tackles a full reliance on these sources

is their fluctuating supply, which requires developing energy storage means with distinctive storage properties. These properties include the high storage-to-volume capability to enable a compact design of the storage unit, the superior thermal properties of the storage material to allow an adequate response rate to the storage and retrieval assignments, and durability of the manufacturing materials to prevent the chemical degradation potential during long operating durations. The latent-heat energy storage (LHES) operated with phase-change materials (PCMs) is considered a compatible scheme for resolving the intermittency issues and supporting a wider utilization of alternative energy sources. LHES is basically a temporary hold of power in the shape of latent heat of fusion for later use. It depends on stimulating the change transition of PCM from solid to liquid (charging) or from liquid to solid (discharging) for energy storage and retrieval, respectively. The key drawback that requires substantial consideration is the low rate of thermal transition during phase transition, owing to the comparatively weak thermal properties of the most present-day PCMs. Some feasible suggestions for resolving the issue involve the proper design of containment system able to deliver a proper thermal transport from the heat transfer fluid (HTF) to the store material, and the application of relevant heat-transfer enhancers such as metal nanoparticles [1–6], fin arrays [7–10], and porous foams [11–15].

In respect to rectifying the weak thermal response arising from the inherent low thermal conductivity of PCMs, the application of fin arrays is recognized as one of the most effective solutions due to their easy integration with the LHES systems and relatively low fabricating costs compared to the other enhancers abovementioned [16]. Studies in the field of LHES applications have demonstrated a growing interest in the implementation of fins for improving the timely thermal response of PCMs to the energy charging and discharging processes. Longitudinal, annular, pin, triangular, and tree-like fins are the configurations examined most in the earlier studies. By employing longitudinal fins, Mat et al. [17] reported 58% and 86% reduction in charging time under the conditions of constant velocity and constant inlet temperature of the HTF, respectively. Rathod and Banerjee [18] reported a reduction of 25% and 44% in PCM melting and solidifying time, respectively, with the inclusion of annular fins in a vertical shell-and-tube heat exchanger. A major improvement was attained applying internal, internal with external, and external triangle fins at 11%, 12%, and 15%, respectively, compared with the cases using longitudinal fins. Abdulateef et al. [19] compared the melting enhancement achieved by triangular fins with longitudinal fins under the same thermal conditions. They concluded that rectangular could provide a faster enhancement rate by up to 15%. To better handle the right dominating role of natural convection during melting, Mahdi et al. [20,21] suggested employing less and smaller fins in the top part of the horizontal LHES units to support better melting enhancement since the melting rate is not the same at the different parts of the unit. Yang et al. [22] showed that the heat transfer improvement by applying annular fins could be better managed if the non-uniform fin distribution in the vertical direction is applied in vertical LHES units.

The previous research has shown that the enhancement potential of thermal performance in LHS systems is largely affected by fins' geometrical configuration. Therefore, some efforts have been performed to examine innovative configurations, for instance Y-configuration fin [23], tree-configuration fin [24], and snowflake-configuration fin [25]. Sciacovelli et al. [23] introduced Y-configuration fins with single and double divisions and suggested that for short operational times, a large angle between branches would be used, while for long operating times, smaller angles are preferable. Pizzolato et al. [26] designed based on topology optimization high conductive fins for the use in small-scale LHS units applicable to district heating applications and reported 37% and 15% faster melting and solidifying rates in topological fins compared to typical longitudinal fins. Yıldız et al. [27] analyzed the melting enhancement of PCMs with various dimensions of tree-shaped rectangular fins and noticed that it could be more effective to optimize the geometrical properties of rectangular fins than employing triangular fins. Yu et al. [28] analysed the melting enhancement of a PCM with tree-configuration fins and found that

the entire charging time can be saved by 27%, and the thermal storage rate can be increased by 45% with ideal tree-configuration fins compared to the conventional fins.

Another important means for improving the thermal response of finned LHS systems is the proper optimization of the various fin design parameters governing the heat transfer and energy storage enhancement rates. These factors involve the fin pitch, number, thickness, and heights of fin at a given volume of the LHS system of concern. Several algorithms for design optimization have been adopted in the literature, including genetic algorithm, particle swarm optimization, and Taguchi method. Because of its relatively easier operation and superior capability for handling multi-dimensional evaluation problems, the Taguchi method has been more broadly utilized in many new experimental and computational works. Taguchi technique has been applied for efficient model assessment of numerous LHS systems [29–34]. For instance, Xie and Yuan [30] employed the Taguchi method to optimize the material and arrangement of the ice thin layer in a cold thermal storage system. Lin et al. [32] optimized the performance of an air-based PCM system using the Taguchi method. Zhang et al. [34] recently achieved a successful fin-geometry optimization via the Taguchi method for better energy-discharging rates in an ice storage unit. Findings of the above studies revealed that the Taguchi method could handle the multi-dimensional optimization problem effectively. Since only the discrete design variables can be handled by the Taguchi method, the results achieved are almost optimal because of its intrinsic optimization characteristics.

Consistent with the ongoing attempts to provide effective solutions for rectifying the poor thermal response of PCMs, this study introduces twisted-tape fins for intensifying the LHS process in a PCM-based shell-and-tube storage unit. Particular attention is paid to the design and optimization of the thermal performance of twisted fins by the Taguchi method. The fin pitch, number of twisted fins, the fin thickness, and the fin height are selected as the main optimal design parameters. A further consideration in this study is paid to the analysis of melting behaviours and heat transfer characteristics in the LHS with optimal twisted fins compared to the LHS unit with conventional longitudinal fins. The data were obtained using the commercially available computational-fluid-dynamic package (ANSYS FLUENT) in connection with a code built in MATLAB for computing of the multiple optimization factors in Taguchi method. A three-dimensional computational model based on finite-volume discretization is developed considering the effects of natural convection in PCM and the temperature-dependent thermal properties of PCM. To our knowledge, no previous research has discussed the impact of twisted fins on the enhancement of PCM thermal response in LHS systems. The study would provide in this regard a distinct benchmark for designing better performing LHS systems applicable to broad engineering applications.

2. Geometry and Boundary Conditions

The proposed system is a double tube LHS equipped with twisted copper fins compared to no-fin and straight fin cases. Figure 1a shows the schematic of the double tube heat exchanger with five twisted fins (attached to the inner tube, which present the heat transfer fluid (HTF) tube), including the boundary conditions and gravity direction. The system is placed vertically, as demonstrated in Figure 1b. Hot water with the uniform inlet temperature of 50 °C and Reynolds number of 1000 is flowed via the central tube, whereas RT35 (PCM) fills the volume of the outer tube considering insulated walls for the PCM container to eliminate the effect of heat loss. A pressure outlet boundary condition is assumed for the outlet surface of the central tube, and a no-slip boundary condition is studied for all the walls. Table 1 shows the properties of the PCM.

(a)   **(b)**
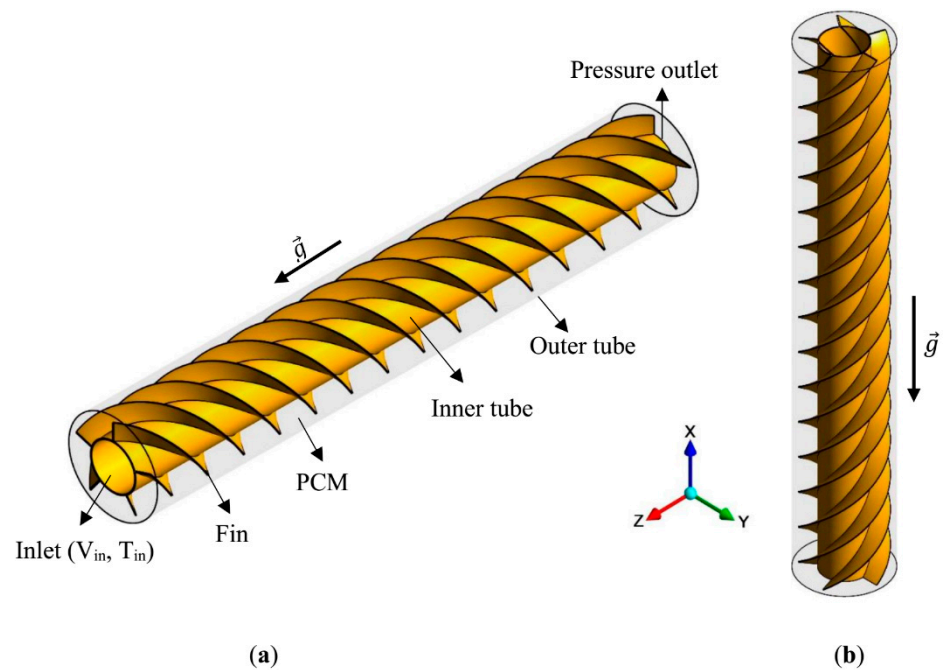
Figure 1. The schematic of the proposed double-tube heat exchanger with twisted fins: (**a**) including **boundary** conditions; (**b**) in vertical placement.

Table 1. Characteristic values of RT35 PCM [35].

Property	μ [N · s/m^2]	β [1/K]	C_p [kJ/kg · K]	k [W/m · K]	ρ [kg/m^3]	L_f [kJ/kg]	T_L [°C]	T_s [°C]
values	0.023	0.0006	2.0	0.2	815	170	35	29

3. Mathematical Modeling

The enthalpy-porosity scheme [35] is implemented to formulate the equations which govern the conservation of mass, momentum, and energy considering the following assumptions [36]:

- Boussinesq approximation for the buoyancy effect.
- The transient, Newtonian, and laminar fluid flow of liquid PCM
- Neglecting viscous dissipation
- Volume expansion is neglected [37]

Conservation of mass:

$$\frac{\partial \rho}{\partial t} + \nabla . \rho \vec{V} = 0, \tag{1}$$

Conservation of momentum:

$$\rho \frac{\partial \vec{V}}{\partial t} + \rho \left(\vec{V} . \nabla \right) \vec{V} = -\nabla P + \mu \left(\nabla^2 \vec{V} \right) - \rho_{ref} \beta \left(T - T_{ref} \right) \vec{g} - A_m \frac{(1-\lambda)^2}{\lambda^3 + 0.001} \vec{V}, \tag{2}$$

Conservation of energy:

$$\frac{\rho C_p \partial T}{\partial t} + \nabla \left(\rho C_p \vec{V} T \right) = \nabla (k \nabla T) - \left[\frac{\partial \rho \lambda L_f}{\partial t} + \nabla \left(\rho \vec{V} \lambda L_f \right) \right] \tag{3}$$

According to the water flow rate in the central tube, the governing equations are considered as the Navier-Stokes equations, which can be accomplished by considering the additional source terms from Equations (2) and (3).

In the above equations, the value of 10^5 kg/m^{3}s was adopted for A_m following the beanchmark studies of [38–40]. The liquid fraction (λ) was introduced using the phase transition temperature as [41]:

$$\lambda = \left\{ \begin{array}{ccc} 0 & if & T < T_{Solidus} \\ \frac{T-T_{Solidus}}{T_{Liquidus}-T_{Solidus}} & if & T_{Solidus} < T < T_{Liquidus} \\ 1 & if & T > T_{Liquidus} \end{array} \right\}, \tag{4}$$

A detailed description of the mathematical model can be found in the authors' previous work [35,42]. The total enthalpy (H) is obtained as:

$$H = \Delta H + h, \tag{5}$$

where:

$$h = \int_{T_{ref}}^{T} C_p dT + h_{ref}, \tag{6}$$

and ΔH was evaluated using $\Delta H = \lambda L_f$. The thermal energy storage rate ($\dot{Q}$) is introduced by the relationship below [43]:

$$\dot{Q} = \frac{Q}{t_m} = \frac{m\left(\int_{solid} c_p dT + L_f + \int_{liquid} c_p dT\right)}{t_m}, \tag{7}$$

4. Numerical Modeling and Validation

The CFD simulation is performed using ANSYS-Fluent 18 employing the QUICK scheme for the diffusion fluxes and convection and PRESTO scheme the pressure correction equation considering 10^{-6} for the convergence. Different mesh and time-step sizes are evaluated as the pre-simulations to find the outcomes separate from the grid density as well as the size of the time step presented in Figure 2. Different cell numbers of 1100 K, 1410 K, and 1940 K are generated for the grid independence analysis. The variations of liquid fraction for different studied cell numbers are illustrated in Figure 2a.
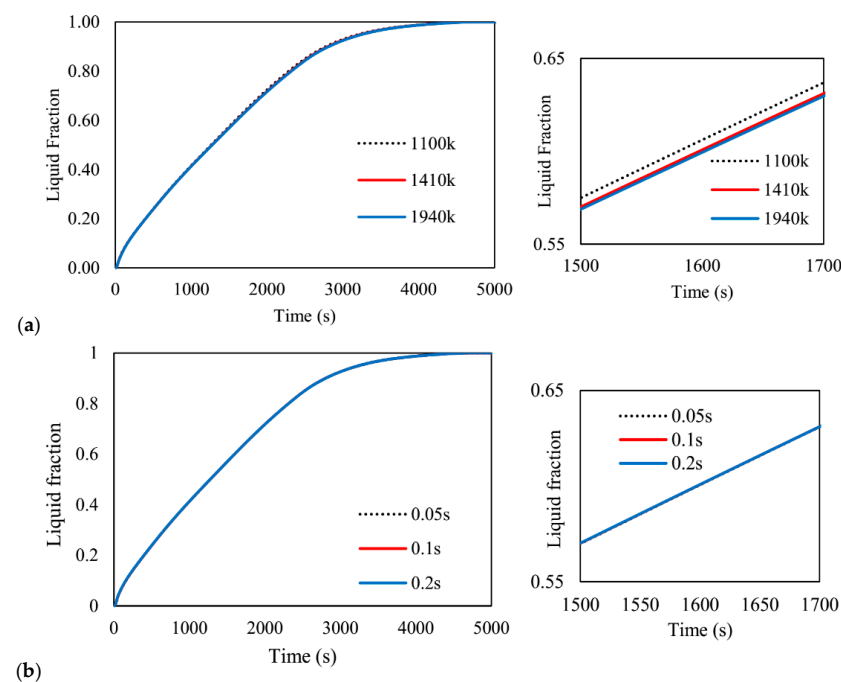
Figure 2. The variations of liquid fraction for different: (**a**) grid numbers; (**b**) time step sizes.

As shown, the results of the cases with the grid numbers of 1410 K and 1940 K are identical, and as a result, the mesh with the grid of the 1410 K cell is chosen for further analysis. For the selected grid, three different time step sizes of 0.05 s, 0.1 s, and 0.2 s are investigated, and the findings are displayed in Figure 2b. As shown, the variations of liquid fraction for all the studied sizes of time step are similar, and therefore, the time step size of 0.2 s was assumed to have less computational time. The configuration of the mesh adopted is illustrated in Figure 3.
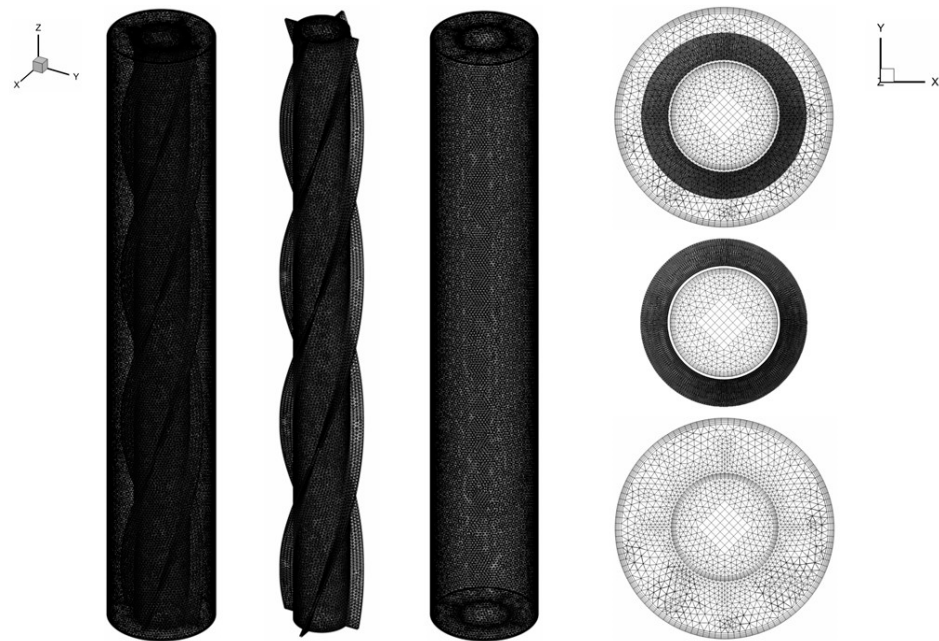

Figure 3. The configuration of the mesh after grid independence analysis.

Verification of the present study is performed in Figure 4 using the numerical and experimental data of Mat et al. [17], which analyzed a charged double pipe LHSHE unit applying RT58 and uniform temperatures on the walls. They examined the presence of inserted fins connected to both internal and external tubes in the PCM container in a staggered configuration. As displayed, a good agreement is found comparing the presented results for both liquid fraction and average temperature with the experimental data and numerical simulations gained from the study of Mat et al. [17].
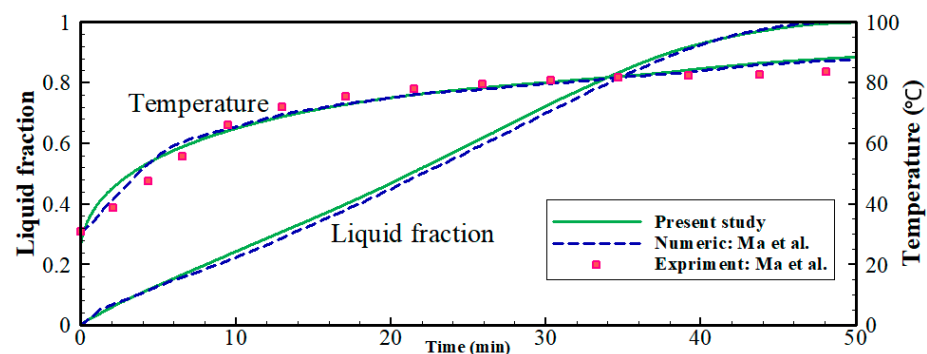

Figure 4. A comparison between the results of the current research and those experimental and numerical data provided by Ma et al. [17].

5. Results and Discussion

5.1. Part A

In this study, different effective parameters of pitch number, number, thickness, and height of the fins are considered as the optimization parameters to find the best performance

gained from the fins' addition. Then, the optimum case will be compared with the system with straight fins and without fins.

The design variables for control of melting heat transfer and thermal energy storage are the fin pitch (1 < Pitch < 3), number of twisted fins (3 < N_{fin} < 5), the fin's thickness (0.5 < t_{fin} < 1.5 mm), and the fins heights (2.5 < H_{fin} < 7.5 mm); all the data are presented in Table 2. Taguchi's technique was adopted to systematically investigate the impact of the design parameters on the *MVF* of the TES unit, as described in Figure 1. The Taguchi method utilizes an orthogonal table of design parameters to probe the design domain. Then, it applies a function evaluation technique to estimate an optimum design. The Taguchi technique has been well established for optimum design experiments involving multiple control variables, influencing the outcomes. Taguchi aims to find an optimum design by performing a minimal number of experiments. In the present study, the Taguchi method is used to maximize the TES unit's output power.

Table 2. The range and levels of control parameters.

Factors	Description	Level 1	Level 2	Level 3
A	*Pitch* (fin's pitch)	1	2	3
B	N_{fin} (number of fins)	3	4	5
C	t_{fin} (mm) (the fin's thickness)	0.5	1	1.5
D	H_{fin} (mm) (fin's height)	2.5	5	7.5

Here, the design of the TES unit involves four control parameters (factors). An arbitrary number of levels can be selected for control parameters. The higher the level number, the more detailed analysis. However, an increase in the levels would intensify the required tests. Here, three levels were selected for each factor. The control parameters and their selected levels are shown in Table 2. All possible combination of four factors leads to 3^4 combination of parameters, which is a big number and demands an expensive and impractical computational cost. Therefore, Taguchi's method proposes the standard orthogonal tables to diminish the essential test while probing the design space. Here, an L9 orthogonal array of factors and parameters was selected and depicted in Table 3. Table 4 proposes nine independent test cases to be examined. These nine cases are adequate to represent the impact of the factors on the design of the TES unit.

Table 3. The Taguchi orthogonal L9 table for the combination of four factors and three levels.

Case	*Pitch*	N_{fin}	t_{fin} (mm)	H_{fin} (mm)	PCM Mass (kg)	Melting Time (s)	Power (W)	SNR
1	1	3	0.5	2.5	0.18676	5072	8.38	18.4649
2	1	4	1	5	0.18369	3690	11.32	21.0769
3	1	5	1.5	7.5	0.17667	2000	19.47	25.7873
4	2	3	1	7.5	0.18314	2689	15.39	23.7448
5	2	4	1.5	2.5	0.18461	4315	9.73	19.7623
6	2	5	0.5	5	0.18508	3071	13.69	22.7281
7	3	3	1.5	5	0.18316	3645	11.43	21.1609
8	3	4	0.5	7.5	0.18402	1943	20.75	26.3404
9	3	5	1	2.5	0.18507	4046	10.40	20.3407
Optimum	3	5	0.5	7.5	0.18388	1675	23.82	-
Straight	-	5	0.5	7.5	0.18386	2864	14.58	-
Without Fin	-	-	-	-	0.18755	5806	7.34	-

Table 4. The rank values of the controlling parameters S/N.

Levels	*Pitch*	N_{fin}	t_{fin} (mm)	H_{fin} (mm)
1	21.78	21.12	22.51	19.52
2	22.08	22.39	21.72	21.66
3	22.61	22.95	22.24	25.29
Delta	0.84	1.83	0.79	5.77
Rank	3	2	4	1

The next step is the simulation of the TES unit and phase change heat transfer for the proposed cases of Table 3. The TES unit's Power at the end of the charging method (*MVF* = 1) was selected as the target design variable, and it was defined as *P* = Stored heat/Melting time. Power (*P*) indicates the capability of the full charging of the unit. The higher the *P*, the better charging performance. After the computation of *P*, an analysis of Signal to Noise Ratio (S/N or SNR) should be performed following the Taguchi method. The SNR indicates the impact of design factors on the heat transfer rate of the TES unit.

The target design of the present investigation is the increase in Power. Thus, the higher-the-better approach was adopted for the Taguchi method. Besides, the impact of factors on the full melting time was estimated using a linear equation and employing the data of Table 4:

$$t\,|_{MVF\,=\,1}\ (\text{s}) = 7597 - 188.0\ Pitch - 381.5\ N_{fin} - 42\ t_{fin} - 453.4\ H_{fin}, \tag{8}$$

Table 3 shows that the variation of design factors notably changes the output power. By using SN ratios and following the Taguchi method, the rank and values of SN ratios were computed and summarized in Table 4. These data are also illustrated in Figure 5. The results show that all factors contribute to charging time and Power of TES; however, their importance of the final Power is not essentially the same. Here, δ values in Table 4 denote the distance between the SN ratios' maximum and a minimum of each factor. The higher the δ value, the stronger the impact of the corresponding factor on Power. Based on computed δ values, the factors were ranked. The last row of Table 4 shows the rank of each factor, and the lower number indicates the most influential factor. Using the last row of Table 4, the influencing factors are as follows $H_{fin} < N_{fin} < Pitch < t_{fin}$. As seen, the height and number of fins are the essential design factors. After these two factors, the fins' pitch and thickness are the second important set of design factors.
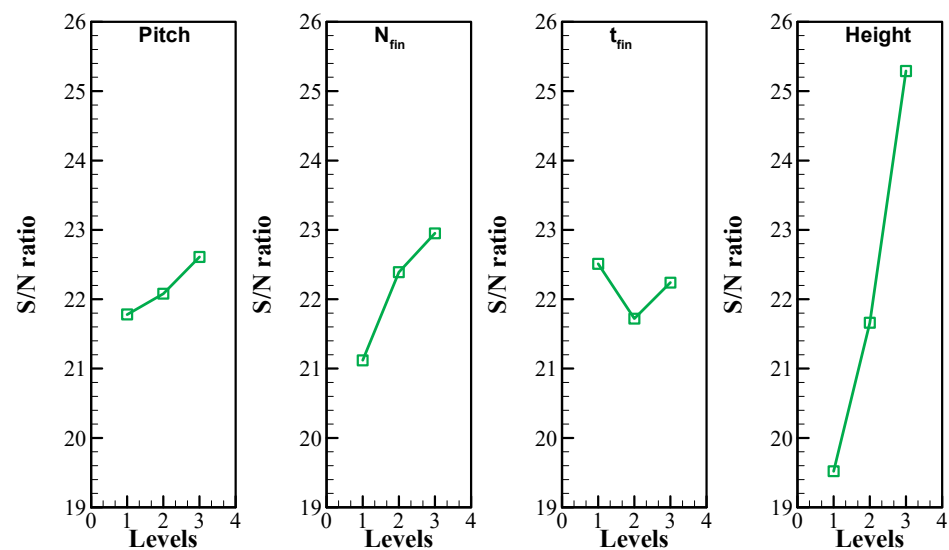

Figure 5. The plot of SN ratios for various design factors and levels. The optimum case for factors of A–D is 3-3-1-3, respectively.

The higher SN ratio always shows the best promising level of a control parameter. Thus, using Figure 5, the highest SN ratios for factors of A–D are 3-3-1-3, respectively. Using the design Table 2, these levels convert to Pitch = 3, N_{fin} = 5, t_{fin} = 0.5 mm, H_{fin} = 7.5 mm. These data are summarized in Table 5. Taguchi's method predicts the optimal Power of P = 21.34 W for this design. The corresponding model of these factors was constructed and simulated. The actual Power of the optimum TES unit was found as P = 23.82 W, which was even higher than the predicted Power. The obtained Power is also higher than all the investigated cases of shown in Table 3. Thus, the design of Table 5 was selected as the final optimum design. The optimum case produces 182% higher charging power compared to a not well-designed case 1 in Table 3. Thus, the optimum design of TES unit could significantly improve its performance.

Table 5. The optimum values of the controlling parameters.

Optimum Factors				Optimum Full Melting Time	
Pitch	N_{fin}	t_{fin} **(mm)**	**Height (mm)**	**Taguchi Prediction**	**Tested Case**
3	5	0.5	7.5	21.34	23.82

The cases of a TES unit with straight fins, with no fins, and optimum design fin are also considered and added to Table 3. These cases do not contribute to the computations of the Taguchi method and were added for the sake of comparison. These cases were also simulated, and the melting time and Power are added to Table 3. Figure 6 displays a system's schematic with three twisted fins with the pitch value of one, which is case 1 from Table 3. Besides, the system with straight fins and without fins are displayed in this figure for the sake of geometrical comparison.

**Case 1**   **Straight case**   **No-fin case**
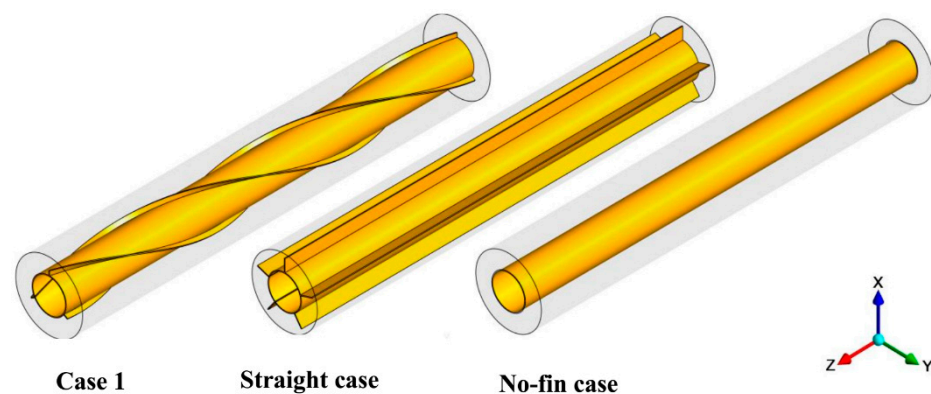
Figure 6. The schematic of double pipe heat storage for case 1, straight fins case, and no-fin case.

The optimum design can provide a charging power of 23.82 W, while the cases of straight fin and without fins produce 14.58 W and 7.34 W. The optimum case could provide 63% higher Power compared to the case of straight fin and 245% higher Power compared to the case of no fin. The mass of PCM has also been reported in Table 3. The mass of PCM is important since the higher mass, the more latent heat energy storage. The optimum TES unit could hold 183.9 g PCM while the cases of straight fin and no fin hold 183.9 and 187.6 g. As seen, the variation of the PCM mass between the optimum fins and straight fins is none. The case with no fin can hold only 2% more PCM mass compared to the optimum case.

Figure 7a shows the stored power in the PCM for all the cases of Taguchi methods. The figure indicates that the optimum case (23.82 W) is higher than the best case (among the nine cases) by 3.07 W, and it is over the worst case (case 1) by 15.44 W. The only difference between the optimum case and case 8 (the best of the nine cases) is the number of the fins, which are 5 and 4 in the optimum case and case 8, respectively. Adding one fin increases the stored power in the system due to the additional surface area of the heat transfer, which

means more heat transfer to the PCM. This concept effect on the charging time of the PCM. The charging rate of the optimum case, case 8, and case 1 are 1675 s, 1943 s, and 5072 s, respectively, as shown in Figure 7b. A system with a fast-melting process could capture high transient thermal loads quickly.

(**a**)

(**b**)
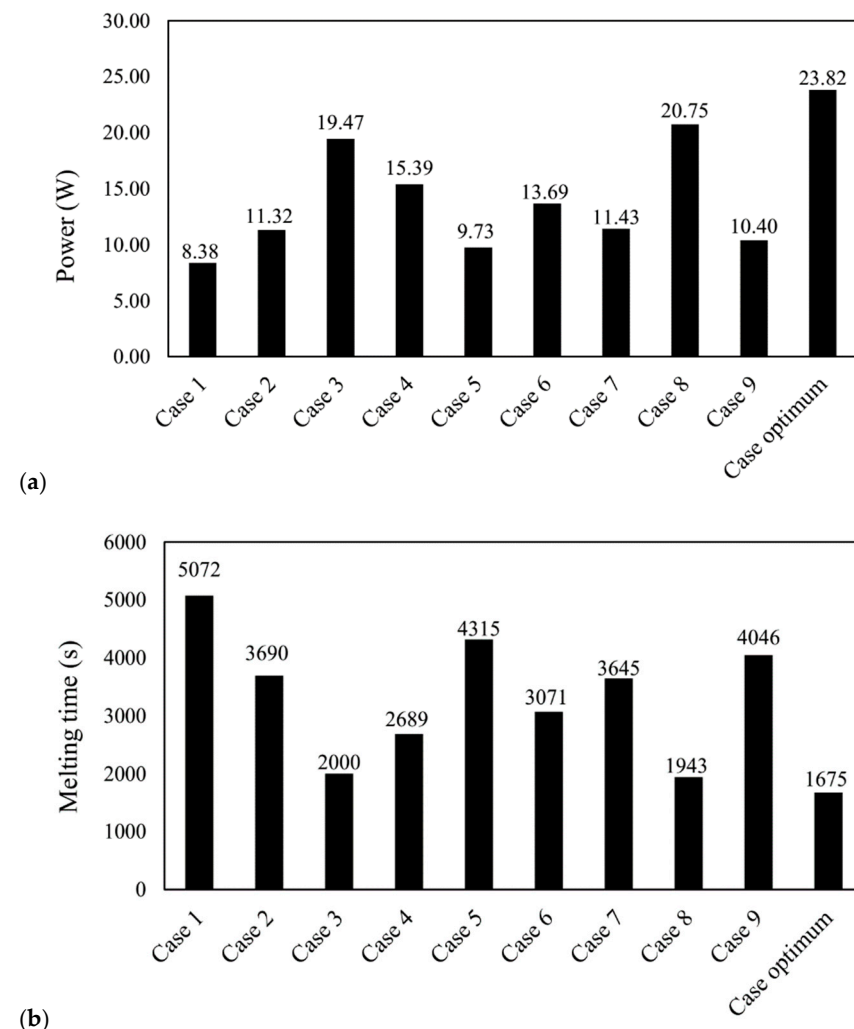
Figure 7. Comparison of all studies cases in the orthogonal Taguchi table: (**a**) the stored power (W); (**b**) the melting time (s).

5.2. Part B

The comparison between the optimum case, and the straight case (with 5 straight fins), and the case without fins illustrates graphically in Figure 8 in terms of the liquid fraction (Figure 8a) and temperature (Figure 8b). Figure 8a shows that the liquid phase of the system without fins increases slightly with a total melting time of 6806 s. The other two cases show the same model for the first 750 s, then the optimum case, which has twisted fins, shows a faster melting time than the straight fins case. This is caused by the twisted fins present a larger surface area and lets more solid parts of the PCM be contacted with the fins surface. It also better guides the molten PCM. These advantages consequently lead to a shorter melting time. Likewise, the presence of fins with different configurations affects the mean temperature of the system. Predictably, the twisted fins help the temperature rise faster, as mentioned because of the large surface area and the slipping effects, helping the molten PCM mix faster. The temperature rises to 50 °C within 2000 s in the optimum case against 3200 s and 6250 s for the straight fins case and the case without fins, respectively.

(**a**)

(**b**)
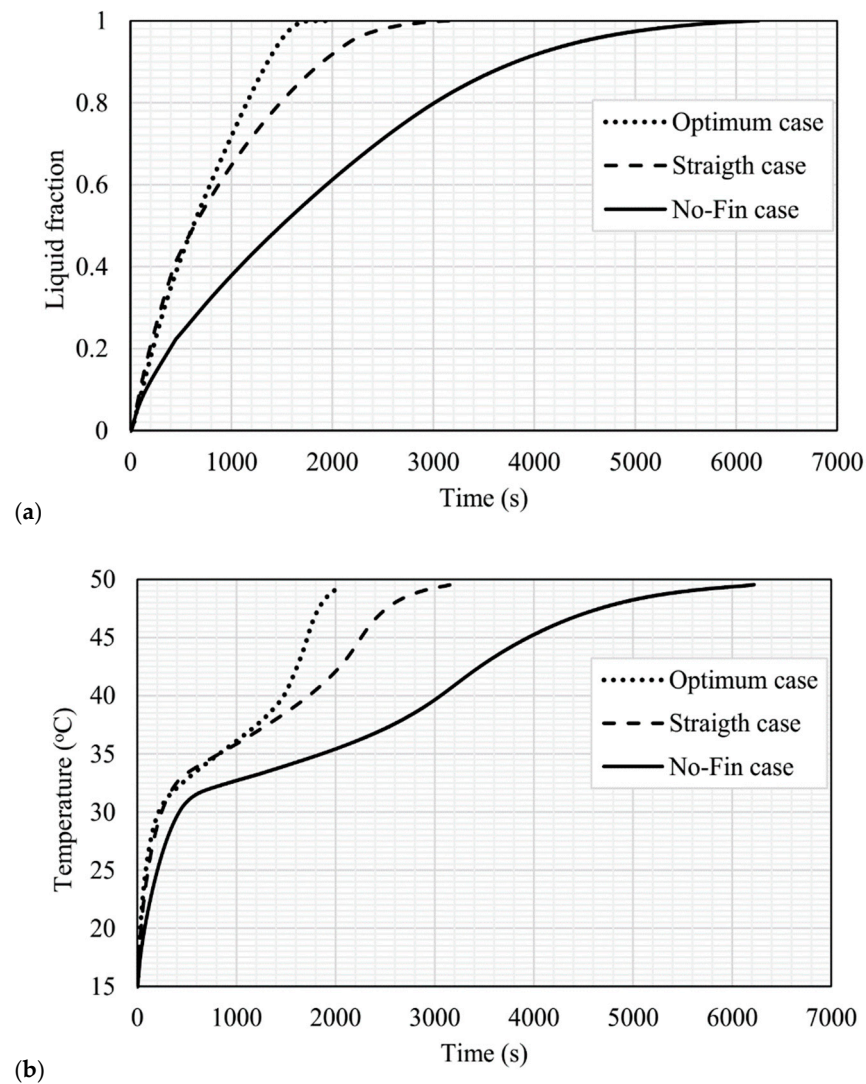
Figure 8. The development of (**a**) the liquid fraction, (**b**) the temperature for the optimum case, straight case (with 5 straight fins, and the case without fins.

The contours of the liquid phase and the thermal parameter for both the optimum and the case without fins are respectively presented in Figure 9a,b. Figure 10a illustrates the liquid development around the HTF tubes and the fins. In the first 600 s the liquid expands faster due to the sufficient thermal management to the PCM, and the solid part is confined between the fins adjacent to the outer tube; then, during the 1800 s, all the PCM malt and the system become ready for the discharging process. However, the HTF generates liquid around the tube only and expands slowly due to the limited thermal capability of PCM material in the system without fins.

Within the 1800 s, the liquid fraction is 50%, and the melting process becomes slower because of the thermal movement through the melted PCM to the solid part. The bottom side of the system melts at the end of the process as the solid part collects at the depth because of the density difference between the two phases of the PCM. The temperature contours (Figure 9b) show that the temperature increases faster in the twisted fins case due to an effective spreading of heat. At 1800 s, most parts of the PCM become in thermal equilibrium with the HTF, except the parts between the fins, adjacent to the outer wall. These parts have a temperature of more than 50 °C, but it is higher than the phase change critical temperature. For the finless case, the close layer of the PCM reaches the thermal equilibrium with the HTF, and the thickness of this layer increases slowly. Within the

1800 s, the temperature of the PCM layer that contacted to the external tube was still the same as the initial temperature, as the heat could not reach there during that time.
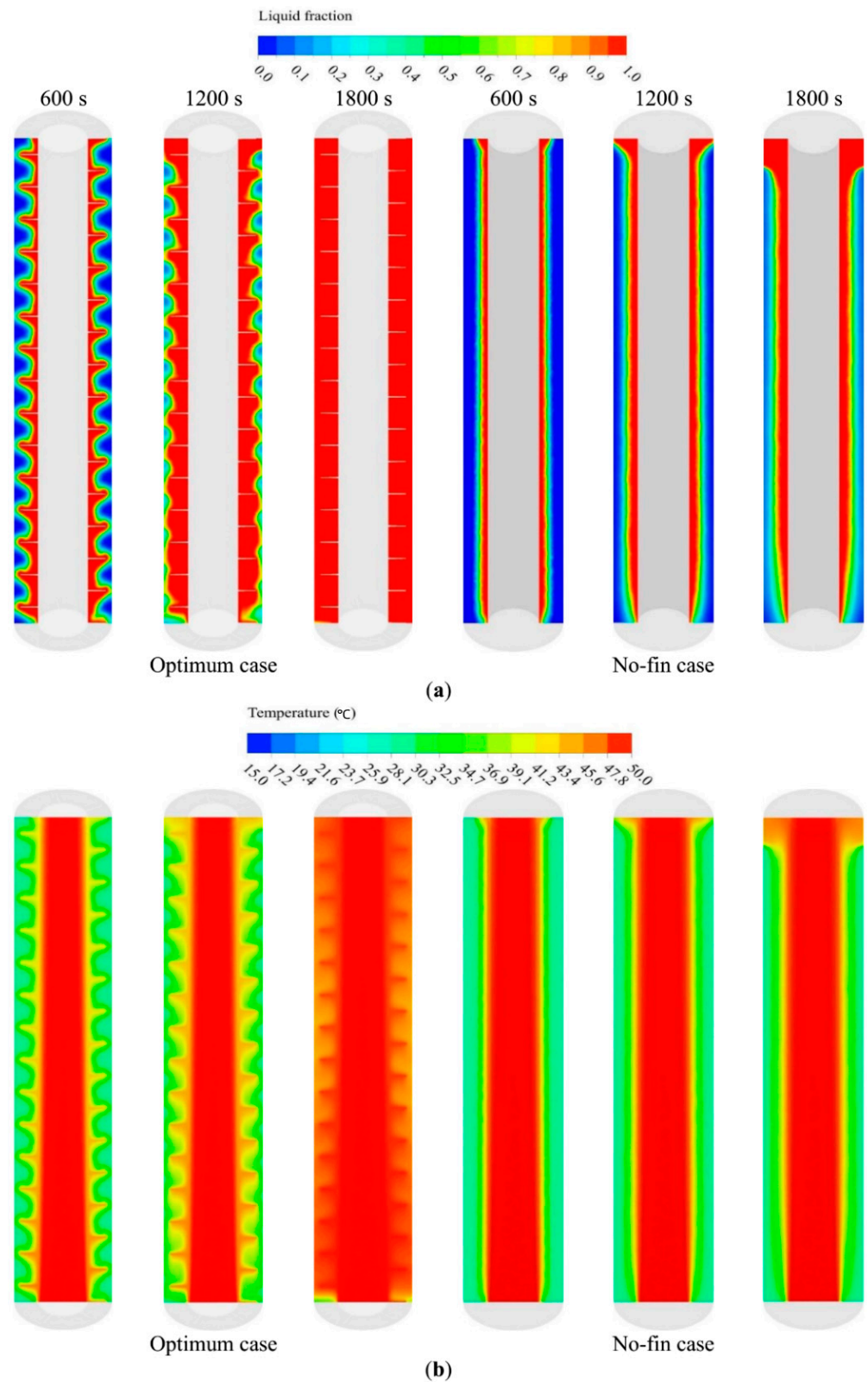
Figure 9. Contours for the optimum case and the case with no fins during 1800 s: (**a**) liquid fraction; (**b**) temperature.
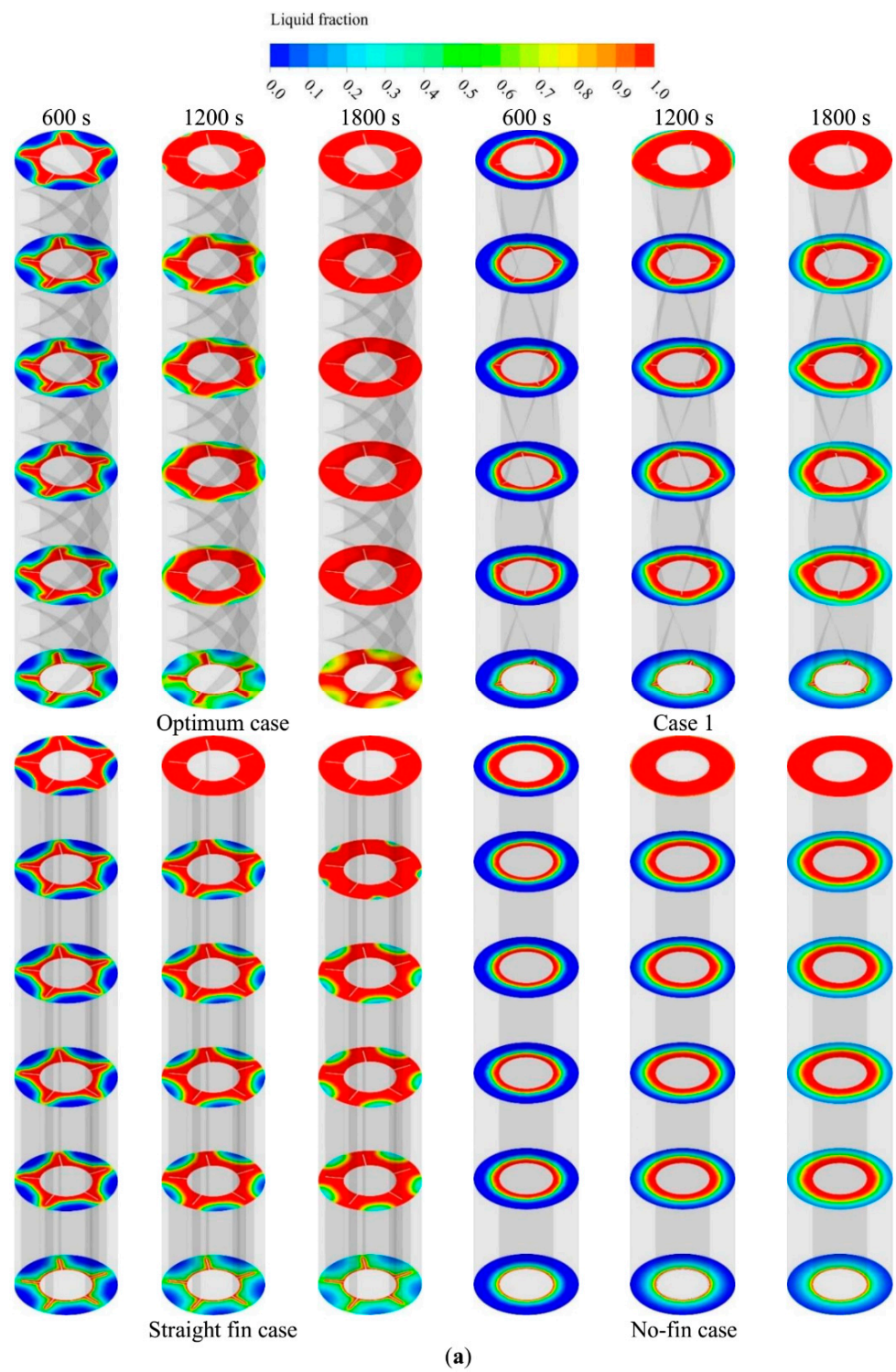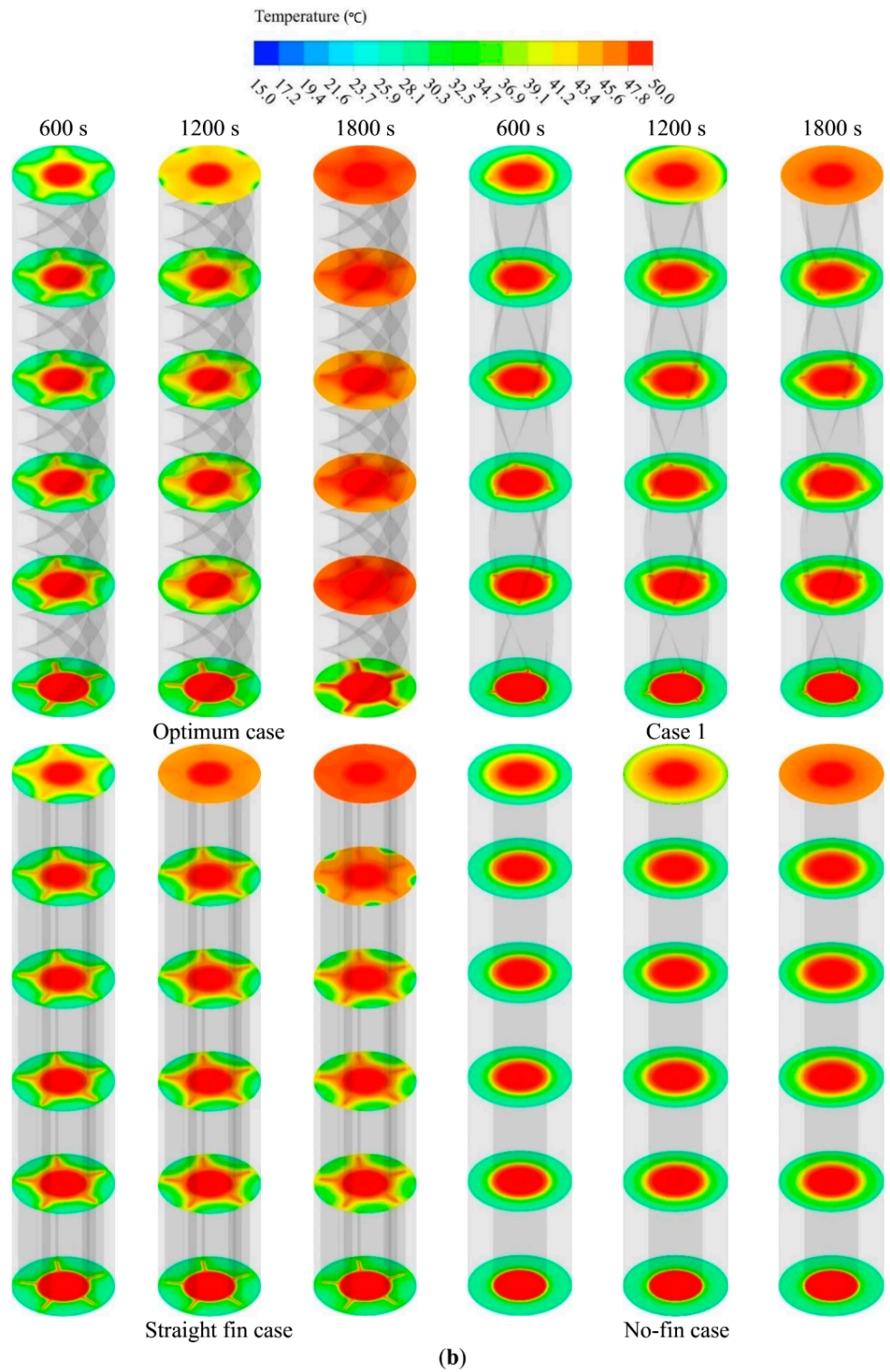
Figure 10. *Cont.*

Figure 10. Development of melting at the different cross-sections for the cases optimum case, case 1, straight fin case, and no-fin case: (**a**) liquid fraction; (**b**) temperature.

Figure 10a shows the liquid fraction at different cross-sections of the optimum case, case 1 (3 fins, 0.5 mm width, 2.5 mm high, and 1 pitch), straight fins case, and finless case. From the optimum case images, it clear that the molten PCM increases wherever risen from the bottom; after 1800 s, there are 0.5% of the PCM not melt at the bottom section of the system. In case 1, the malt PCM is less than the optimum, and the development of the liquid PCM reaches 45% within 1800 s. The huge difference between the optimum case and

case 1 in terms of melting process and temperature distribution is caused by the number, size, and configurations of the fins. With the straight fins, the molten PCM is more than case 1 (even in case 1, the fins are twisted). This is because of the greater number of the fins and the large surface area, which helps more energy passes to the PCM. The absence of the fin leaves the majority of the PCM not molten (65%) after 1800 s as the heat transfers to the PCM through the internal wall (HTF tube). The temperature steps the same mode as the liquid fractions shown in Figure 10b. The optimum case arrives at the equilibrium state in all the cross-sections except the bottom section, which still has some patch (between the fins) in lower temperature. The PCM in case1 arrives 48 °C at the top section but still cold as the initial temperature on the bottom section. The star shape patches clearly appear in the middle sections of the system with the straight fins. However, the ring patches appear in the finless system with an average temperature of 37 °C.

Figure 11 shows the distribution of Fins temperature at different times. Because of the flowing of the hot water from the base part of the heat exchanger, a higher temperature can be seen at the bottom of the domain compared with the top area. Moreover, through time, the difference between the temperature at the bottom and top sides of the domain increases. For example, after 600s, the major temperature difference in the fins is almost 6 °C while almost 2.5 °C after 1800 s. The reason is that the rate of heat storage by the PCM reduces through time, and due to the insulated surface of the outer wall, the rate of thermal exchange between the HTF to the PCM by the fins decreases and consequently, a more uniform temperature distribution is achieved in the domain.
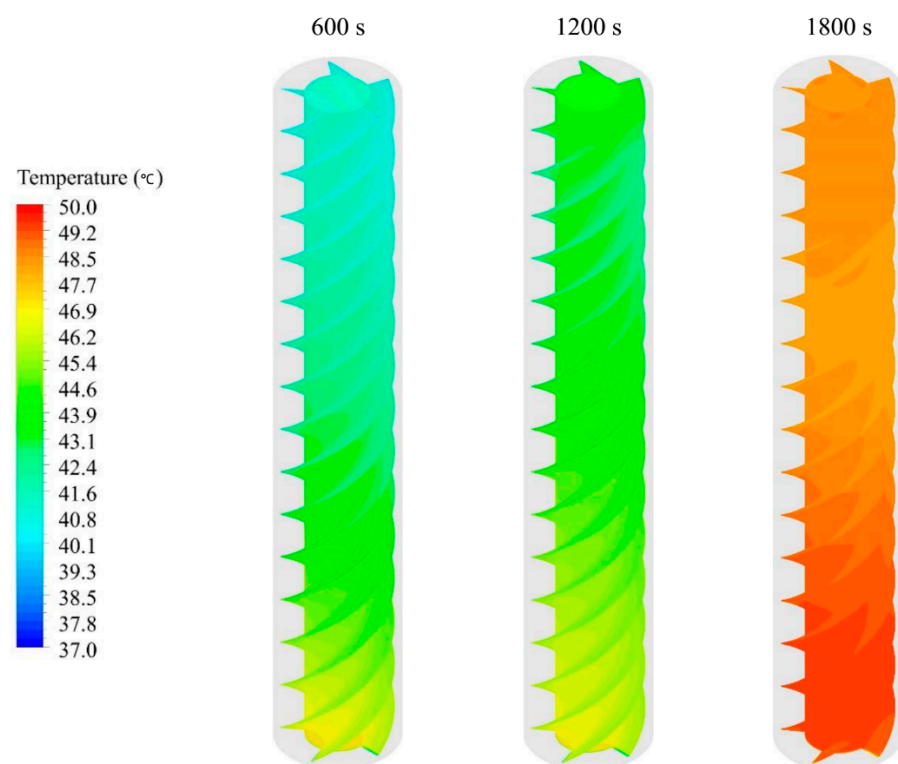
Figure 11. Temperature profile for the HTF tube and the fins in the optimum case at different time steps.

Figure 12 shows the temperature of the HTF in the internal tube at different times. At the time 600 s, the HTF is warm at the bottom section (as an initial condition), the temperature becomes colder at the adjacent region to the wall; this is because the fluid losses heat to the PCM. At the 1200 s, the PCM becomes warmer, then the transfer heat to the PCM drops due to the temperature difference between the PCM and the HTF drops. This makes the HTF lose less heat than the 600 s. This concept clearly appears in 1800 s,

in which the HTF temperature at the outer section is extremely close to the inlet section, meaning that the PCM gains much less heat than earlier time.
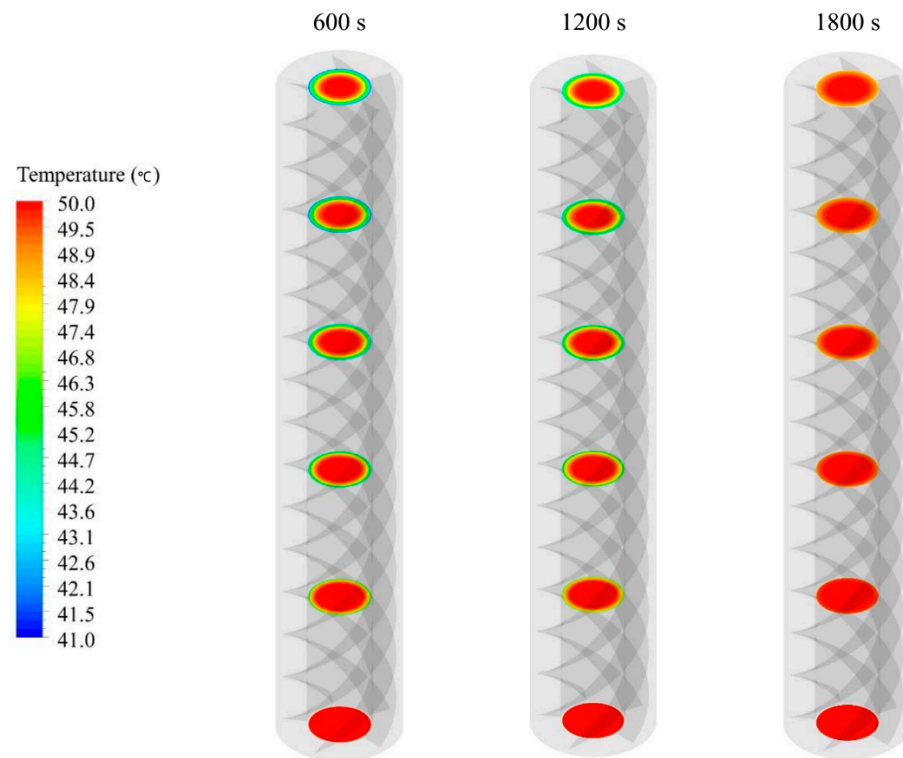
Figure 12. Temperature profile for the HTF at different cross-sections in the optimum case at different time steps.

6. Conclusions

A twisted-fin array as an efficient enhancer for boosting better charging response in the poor thermally conductive PCM-based heat storage systems was applied and numerically analyzed in this research. A three-dimensional model simulating the transient two-phase flow and thermal associated with the charging of PCM was developed and verified via previous related experiments.

Twelve different case studies were examined to explore the effects of fin shape factors such as the fin pitch, number, thickness, and height of the twisted fin on the overall energy charge process. Optimization of these parameters to reach the optimal fin design was conducted via the Taguchi method. The numerical results were presented in the form of temporal temperature distribution, melting front evolution, melting time, and energy storage rate and discussed. The results showed that the energy charging time could be reduced by about 6 to 42% depending on twisted fins' geometric parameters. The energy storage rate could be enhanced by about 6 to 63% compared to the reference case of straight longitudinal fins within the same PCM mass limitations. The comparison also showed that optimizing the twisted fin parameter is an effective strategy towards constructing an appropriate design to enhance the charge efficiency of the PCM-based heat storage units and extend their applications. In the future studies, the authors are planning to investigate the wider range of studied parameters, the effects of the utilized materials and the orientation of the tubes. Moreover, with the help of additive manufacturing, the authors are planning to fabricate the studied geometry and experimentally investigate the twisted fin effects.

Abbreviations

Nomenclature

A_m	Constant for mush source term	$t_m(s)$	Melting time
C_p (Jkg^{-1}K^{-1})	Specific heat capacity	T (K)	Temperature
g (ms^{-2})	Gravity	T_e(K)	End temperature
H (kJ/mol)	Enthalpy	T_i (K)	Initial temperature
H_{fin} (mm)	Height of fins	T_{in} (K)	Inlet temperature
k (Wm^{-1}K^{-1})	Thermal conductivity	$\overrightarrow{V}$ (m/s)	Velocity
LF	Liquid fraction–Melt fraction	$\overrightarrow{V}_{in}$ (m/s)	Inlet velocity
N_{fin}	Number of fins		
m (kg)	Mass	**Greek symbols**	
P (W)	Power	β (K^{-1})λ	Expansion coefficient
$Pitch$	Fin's pitch	$\lambda\mu$ (kgm^{-1}s^{-1})	Expansion coefficient
Q (J)	Capacity of heat storage	μ (kgm^{-1}s^{-1})ρ (kgm^{-3})	Liquid fraction
$\dot{Q}$ (W)	Rate of stored heat	ρ (kgm^{-3})ΔH (Jkg^{-1})	Dynamic Viscosity
t_{fin} (mm)	Thickness of fins	ΔH (Jkg^{-1})	Density
T_L (K)	Temperature (Liquidus)		Stored latent heat energy
T_s (K)	Temperature (Solidus)		

References

1. Liao, Z.; Xu, C.; Ren, Y.; Gao, F.; Ju, X.; Du, X. A novel effective thermal conductivity correlation of the PCM melting in spherical PCM encapsulation for the packed bed TES system. *Appl. Therm. Eng.* **2018**. [CrossRef]
2. Al-Jethelah, M.; Tasnim, S.H.; Mahmud, S.; Dutta, A. Nano-PCM filled energy storage system for solar-thermal applications. *Renew. Energy* **2018**. [CrossRef]
3. Ebadi, S.; Tasnim, S.H.; Aliabadi, A.A.; Mahmud, S. Melting of nano-PCM inside a cylindrical thermal energy storage system: Numerical study with experimental verification. *Energy Convers. Manag.* **2018**, *166*, 241–259. [CrossRef]
4. Mahdi, J.M.; Nsofor, E.C. Solidification of a PCM with nanoparticles in triplex-tube thermal energy storage system. *Appl. Therm. Eng.* **2016**, *108*, 596–604. [CrossRef]
5. Mahdi, J.M.; Nsofor, E.C. Melting of PCM with Nanoparticles in a Triplex-Tube Thermal Energy Storage System. *Ashrae Trans.* **2016**, *122*, 215–224.
6. Shanan, Z.J.; Hadi, S.M.; Shanshool, S.K. Structural analysis of chemical and green synthesis of cuo nanoparticles and their effect on biofilm formation. *Baghdad Sci. J.* **2018**, *15*, 211–216. [CrossRef]
7. Sheikholeslami, M.; Lohrasbi, S.; Ganji, D.D. Numerical analysis of discharging process acceleration in LHTESS by immersing innovative fin configuration using finite element method. *Appl. Therm. Eng.* **2016**, *107*, 154–166. [CrossRef]
8. Lohrasbi, S.; Sheikholeslami, M.; Ganji, D.D. Discharging process expedition of NEPCM in fin-assisted latent heat thermal energy storage system. *J. Mol. Liq.* **2016**, *221*, 833–841. [CrossRef]
9. Mahdi, J.M.; Nsofor, E.C. Melting enhancement in triplex-tube latent thermal energy storage system using nanoparticles-fins combination. *Int. J. Heat Mass Transf.* **2017**, *109*, 417–427. [CrossRef]
10. Mahdi, J.M.; Nsofor, E.C. Solidification enhancement of PCM in a triplex-tube thermal energy storage system with nanoparticles and fins. *Appl. Energy* **2018**, *211*, 975–986. [CrossRef]

11. Deng, Z.; Liu, X.; Zhang, C.; Huang, Y.; Chen, Y. Melting behaviors of PCM in porous metal foam characterized by fractal geometry. *Int. J. Heat Mass Transf.* **2017**, *113*, 1031–1042. [CrossRef]

12. Mahdi, J.M.; Nsofor, E.C. Melting enhancement in triplex-tube latent heat energy storage system using nanoparticles-metal foam combination. *Appl. Energy* **2017**, *191*, 22–34. [CrossRef]

13. Mahdi, J.M.; Nsofor, E.C. Solidification enhancement in a triplex-tube latent heat energy storage system using nanoparticles-metal foam combination. *Energy* **2017**, *126*, 501–512. [CrossRef]

14. Mahdi, J.M.; Mohammed, H.I.; Hashim, E.T.; Talebizadehsardari, P.; Nsofor, E.C. Solidification enhancement with multiple PCMs, cascaded metal foam and nanoparticles in the shell-and-tube energy storage system. *Appl. Energy* **2020**, *257*, 113993. [CrossRef]

15. Mohammed, H.I.; Talebizadehsardari, P.; Mahdi, J.M.; Arshad, A.; Sciacovelli, A.; Giddings, D. Improved melting of latent heat storage via porous medium and uniform Joule heat generation. *J. Energy Storage* **2020**, *31*, 101747. [CrossRef]

16. Abdulateef, A.M.; Mat, S.; Abdulateef, J.; Sopian, K.; Al-Abidi, A.A. Geometric and design parameters of fins employed for enhancing thermal energy storage systems: A review. *Renew. Sustain. Energy Rev.* **2018**, *82*, 1620–1635. [CrossRef]

17. Mat, S.; Al-Abidi, A.A.; Sopian, K.; Sulaiman, M.Y.; Mohammad, A.T. Enhance heat transfer for PCM melting in triplex tube with internal–external fins. *Energy Convers. Manag.* **2013**, *74*, 223–236. [CrossRef]

18. Rathod, M.K.; Banerjee, J. Thermal performance enhancement of shell and tube Latent Heat Storage Unit using longitudinal fins. *Appl. Therm. Eng.* **2015**, *75*, 1084–1092. [CrossRef]

19. Abdulateef, A.M.; Mat, S.; Sopian, K.; Abdulateef, J.; Gitan, A.A. Experimental and computational study of melting phase-change material in a triplex tube heat exchanger with longitudinal/triangular fins. *Sol. Energy* **2017**, *155*, 142–153. [CrossRef]

20. Mahdi, J.M.; Lohrasbi, S.; Ganji, D.D.; Nsofor, E.C. Accelerated melting of PCM in energy storage systems via novel configuration of fins in the triplex-tube heat exchanger. *Int. J. Heat Mass Transf.* **2018**, *124*, 663–676. [CrossRef]

21. Mahdi, J.M.; Lohrasbi, S.; Ganji, D.D.; Nsofor, E.C. Simultaneous energy storage and recovery in the triplex-tube heat exchanger with PCM, copper fins and Al2O3 nanoparticles. *Energy Convers. Manag.* **2019**, *180*, 949–961. [CrossRef]

22. Yang, X.; Guo, J.; Yang, B.; Cheng, H.; Wei, P.; He, Y.-L. Design of non-uniformly distributed annular fins for a shell-and-tube thermal energy storage unit. *Appl. Energy* **2020**, *279*, 115772. [CrossRef]

23. Sciacovelli, A.; Gagliardi, F.; Verda, V. Maximization of performance of a PCM latent heat storage system with innovative fins. *Appl. Energy* **2015**, *137*, 707–715. [CrossRef]

24. Zhang, C.; Li, J.; Chen, Y. Improving the energy discharging performance of a latent heat storage (LHS) unit using fractal-tree-shaped fins. *Appl. Energy* **2020**, *259*, 114102. [CrossRef]

25. Konan, H.C.; Cetkin, E. Snowflake shaped high-conductivity inserts for heat transfer enhancement. *Int. J. Heat Mass Transf.* **2018**, *127*, 473–482. [CrossRef]

26. Pizzolato, A.; Sharma, A.; Maute, K.; Sciacovelli, A.; Verda, V. Design of effective fins for fast PCM melting and solidification in shell-and-tube latent heat thermal energy storage through topology optimization. *Appl. Energy* **2017**, *208*, 210–227. [CrossRef]

27. Yıldız, Ç.; Arıcı, M.; Nižetić, S.; Shahsavar, A. Numerical investigation of natural convection behavior of molten PCM in an enclosure having rectangular and tree-like branching fins. *Energy* **2020**, *207*, 118223. [CrossRef]

28. Yu, C.; Wu, S.; Huang, Y.; Yao, F.; Liu, X. Charging performance optimization of a latent heat storage unit with fractal tree-like fins. *J. Energy Storage* **2020**, *30*, 101498. [CrossRef]

29. Lin, W.; Ma, Z. Using Taguchi-Fibonacci search method to optimize phase change materials enhanced buildings with integrated solar photovoltaic thermal collectors. *Energy* **2016**, *106*, 23–37. [CrossRef]

30. Xie, J.; Yuan, C. Parametric study of ice thermal storage system with thin layer ring by Taguchi method. *Appl. Therm. Eng.* **2016**, *98*, 246–255. [CrossRef]

31. Ren, H.; Lin, W.; Ma, Z.; Fan, W.; Wang, X. Thermal performance evaluation of an integrated photovoltaic thermal-phase change material system using Taguchi method. *Energy Procedia* **2017**, *121*, 118–125. [CrossRef]

32. Lin, W.; Ma, Z.; Ren, H.; Gschwander, S.; Wang, S. Multi-objective optimisation of thermal energy storage using phase change materials for solar air systems. *Renew. Energy* **2019**, *130*, 1116–1129. [CrossRef]

33. Kolioak, Y.; Radhakrishna, M.; Prasad, A. Optimization of Heat Energy Based on Phase Change Materials used in Solar Collector using Taguchi Method. *Mater. Today Proc.* **2020**, *22*, 2404–2411. [CrossRef]

34. Zhang, C.; Sun, Q.; Chen, Y. Solidification behaviors and parametric optimization of finned shell-tube ice storage units. *Int. J. Heat Mass Transf.* **2020**, *146*, 118836. [CrossRef]

35. Talebizadeh Sardari, P.; Walker, G.S.; Gillott, M.; Grant, D.; Giddings, D. Numerical modelling of phase change material melting process embedded in porous media: Effect of heat storage size. *Proc. Inst. Mech. Eng. Part A J. Power Energy* **2019**. [CrossRef]

36. Shahsavar, A.; Majidzadeh, A.H.; Mahani, R.B.; Talebizadehsardari, P. Entropy and Thermal performance Analysis of PCM Melting and Solidification Mechanisms in a Wavy Channel Triplex-Tube Heat Exchanger. *Renew. Energy* **2021**. [CrossRef]

37. Talebizadehsardari, P.; Mohammed, H.I.; Mahdi, J.M.; Gillott, M.; Walker, G.S.; Grant, D.; Giddings, D. Effect of airflow channel arrangement on the discharge of a composite metal foam-phase change material heat exchanger. *Int. J. Energy Res.* **2020**. [CrossRef]

38. Ye, W.-B.; Zhu, D.-S.; Wang, N. Numerical simulation on phase-change thermal storage/release in a plate-fin unit. *Appl. Therm. Eng.* **2011**, *31*, 3871–3884. [CrossRef]

39. Assis, E.; Katsman, L.; Ziskind, G.; Letan, R. Numerical and experimental study of melting in a spherical shell. *Int. J. Heat Mass Transf.* **2007**, *50*, 1790–1804. [CrossRef]

40. Sardari, P.T.; Giddings, D.; Grant, D.; Gillott, M.; Walker, G.S. Discharge of a composite metal foam/phase change material to air heat exchanger for a domestic thermal storage unit. *Renew. Energy* **2019**. [CrossRef]
41. Al-Abidi, A.A.; Mat, S.; Sopian, K.; Sulaiman, M.Y.; Mohammad, A.T. Internal and external fin heat transfer enhancement technique for latent heat thermal energy storage in triplex tube heat exchangers. *Appl. Therm. Eng.* **2013**, *53*, 147–156. [CrossRef]
42. Shahsavar, A.; Goodarzi, A.; Mohammed, H.I.; Shirneshan, A.; Talebizadehsardari, P. Thermal performance evaluation of non-uniform fin array in a finned double-pipe latent heat storage system. *Energy* **2020**, *193*, 116800. [CrossRef]
43. Xu, Y.; Ren, Q.; Zheng, Z.-J.; He, Y.-L. Evaluation and optimization of melting performance for a latent heat thermal energy storage unit partially filled with porous media. *Appl. Energy* **2017**, *193*, 84–95. [CrossRef]